NINTH EUROPEAN ROTORCRAFT FORUM

Paper No. 47

DESIGN AND DEVELOPMENT OF A COMPOSITE MAIN ROTOR BLADE FOR THE Y-2 HELICOPTER

ZHANG CHENGLIN ZHANG XIAOGU

Nanjing Aeronautical Institute

(Nanjing)

People's Republic of China

September 13—15, 1983

STRESA, ITALY

Associazione Industrie Aerospaziali

Associazione Italiana di Aeronautica ed Astronautica

DESIGN AND DEVELOPMENT OF A COMPOSITE MAIN ROTOR BLADE FOR THE Y-2 HELICOPTER

Zhang Chenglin, Zhang Xiaogu
Nanjing Aeronautical Institute
Nanjing, People's Republic of China

ABSTRACT

A program for the design and development of a new composite main rotor blade for the Y-2 helicopter was initiated in 1977 at our Institute. Since then we have undertaken a large amount of design work and an extensive series of tests to evaluate the properties of the blade. These tests include: aeordynamic test, structural test, dynamic test, fatigue test, ground tie-down test, etc. From the results of the program we found that there are substantial improvements in the aerodynamic performance,dynamic property and fatigue strength over the metal blade previously installed on the Y-2 helicopter. The experiments indicate that the calculated bending stiffness and bending natural frequency are in good agreement with the measured data. We have also included a new technique for detemining the rotor-body coupled natural frequencies through the combination of analyses and test data by the mechanical impedance method.

1. Introduction

The Y-2 helicopter is a light weight vehicle designed and developed during 1967 to 1975 by Nanjing Aeronautical Institute (ref.). In its original version, composite materials were used for several components, such as:

Fig.1 Y-2 Helicopter in Flight

the tail rotor blade skin and the cabin door, etc, but the main rotor blade is still made of metal construction. In 1977 we collaborated with Beijing Aeronautical Institute and factories to initiate a program for developing a composite main rotor blade to replace the vehicle's original metal blade. In this project we undertook the design and ground test work.

The list of basic requirements for the design and development of the blade are as follows:

1) Retrofit the new blade to the existing helicopter.
2) Improved hover performance.
3) Satisfactory dynamic properties.
4) Significant improvement in fatigue life.

2. Blade Geometry and Aerodynamics

Due to its ease in moulding and high fatigue strength, a composite blade has much higher geometric freedom when compared with a metal blade. We, therefore, decided to modify the geometry of the new blade so as to meet the requirement for an improved hover performance. The modified blade geometry is shown in Table.1 and Figure 1, together with that of the original metal blade for comparison.

Table 1 Blade Geometry

	Composite Blade	Metal Blade
Radius m	5	5
Rotational Speed R.P.M	357.9	357.9
Number of Blades	3	3
Solidity	0.04645	0.0489
Taper Ratio	1.2	1
Twist deg.	−8	−5.5
Airfoil	unsymmetrical	C012

The major changes in the design of the composite blade's geometry are: unsymmetrical airfoil (modified from C012) , increased negative twist, tapered planform, decreased solidity.

All of these changes are beneficial to hovering efficiency. Due to the higher maximum lift coefficient of the modified airfoil, the solidity can be reduced in some extent to decrease the profile power. While the tapered planform is not only advantageous to performance but also beneficial to the dynamic property (1st flapwise natural frequency) and blade static

droop.

The modified unsymmetrical airfoil was investigated in a two-dimensional windtunnel test to evaluate its aerodynamic charateristics. The result is satisfactory.

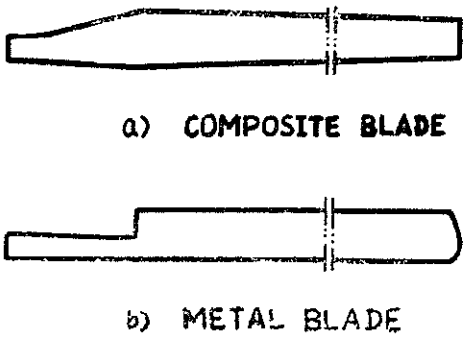

Fig.2 Planform of Composite Blade and Metal Blade

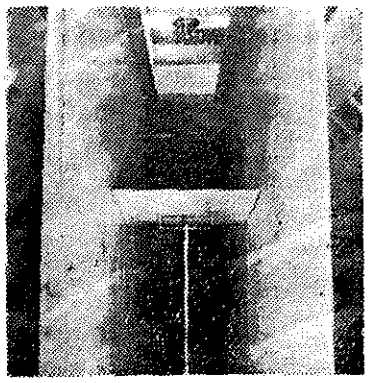

Fig.3 Airfoil Windtunnel Test

Through the improvement of the blade geometry, the hover ceiling (OGE) is increased by about 800 m, or the rotor thrust increased by about 50 kg.

3. Construction and Material

The blades consists of a front "C" spar, trailingedge strip, outerskin, foam core, erosion shield and nose balance weight.

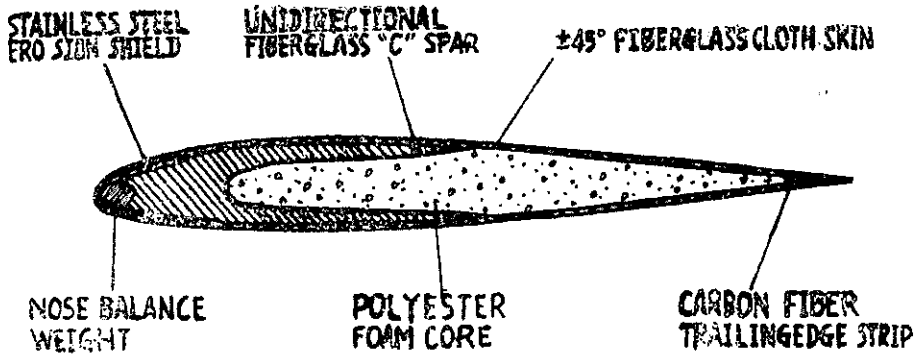

Fig.4 Y-2 Composite Blade Configuration

The spanwise oriented unidirectional S glass fiber was chosen for the spar to attain the required flapwise bending stiffness and strength, tensile strength. The skin consists of six layers of S glass cloth oriented at ±45° to attain the required torsional stiffness. The carbon fiber trailing edge strip is usd to increase the chordwise bending stiffness. According to

the original design, the skin consists of only four layers of glass cloth and the trailingedge strip is made also from fiber glass, and later on the number of the skin layers was increased to six to improve the torsional stiffness. As a consequence of this design change, the material of the trailingedge strip also had to be changed to carbon fiber to avoid chordwise bending mode resonance in the final configuration.

Figure 5 shows the details of the blade root end construction. Because of the requirement that the blade should be a retrofit to the existing helicopter, especially to the rotor hub, it is necessary to use a metal fitting

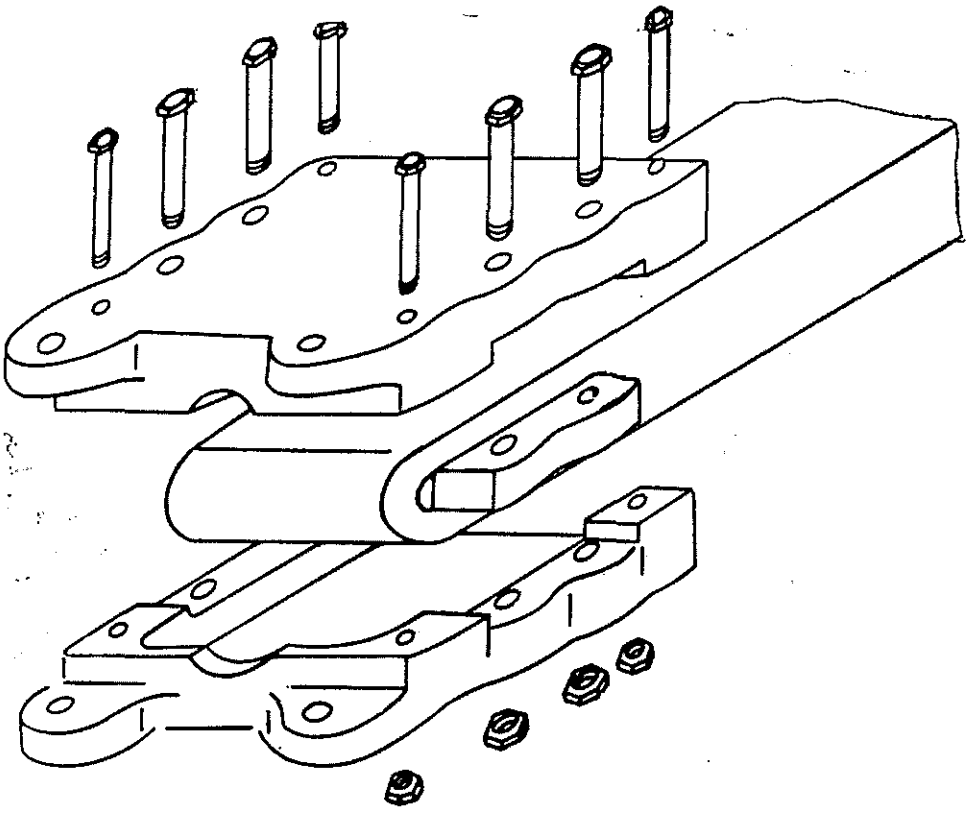

Fig.5 Y-2 Composite Blade Root End Construction

to connect the blade and the hub. This is accomplished by inserting a short horizontal beam into the fiberglass root end of the "C" spar, and set this combination (consisting of the spar root end and the short beam) between the lower and upper halves of the metal fitting. The assemblage is then fastened together by a set of bolts and nuts.

Mechanical properties of the composite blade material are listed in Table 2.

Table.2 Properties of Blade Material

Material	S Glass, 0° (spar)	S Glass, ±45° (skin)	Carbon, 0°
Resin Ratio %	27.3	32.5	
Density g/cm³	1.91	1.86	1.61
Ultimate Bending Strength kg/cm²	11600	4100	13200
Ultimate Tensile Strength kg/cm²	10500	3680	12000
Bending Modulus kg/cm² × 10⁵	4.05	1.66	8.89
Tensile Modulus kg/cm² × 10⁵	4.16	1.82	10.1
Shear Strength kg/cm²	690		
Shear Modulus kg/cm² × 10⁵		1.18	

4. Mass and Mass Distribution

Table. 3 shows the mass characteristics of the composite blade compared with the original metal blade.

Table.3 Mass Characteristics of Blade

	Composite Blade	Metal Blade
Flapping Mass Inertia, kg-m-sec²	21.742	19.515
Flapping Mass Moment, kg-sec²	7.0145	6.67
Blade Total Weight, kg	28	27

The mass distribution of the composite blade and metal blade is shown in Figure.6.

It is evident that the mass characteristics of the composite blade are nearly the same as the original metal blade, thus the excellent handling quality of the Y-2 helicopter with metal blade can be maintained.

The chordwise center of gravity distribution is shown in Figure. 7.

The effective relative chordwise C.G position $\bar{\sigma}e^*$ equal to 0.247 from leading edge, slightly forward of the quarter chord.

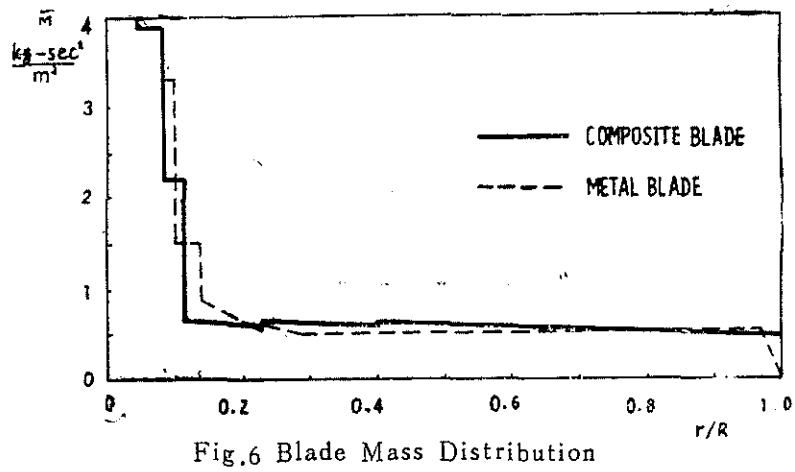

Fig.6 Blade Mass Distribution

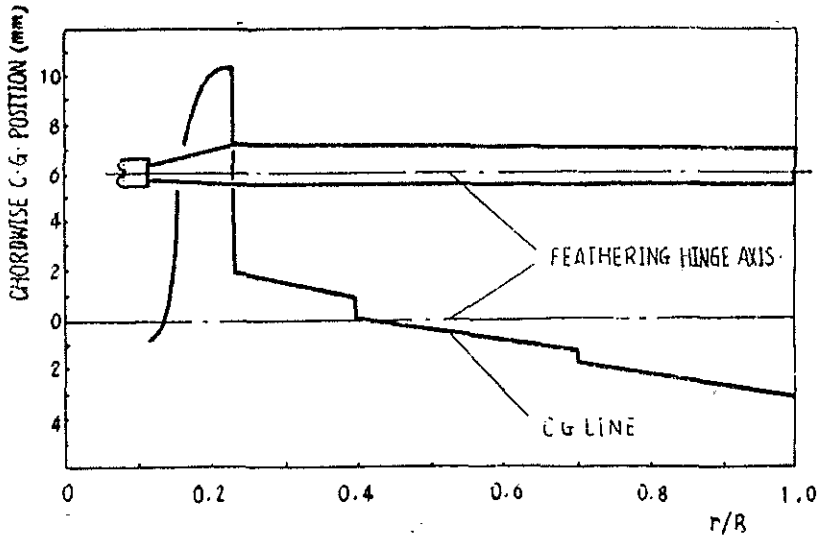

Fig.7 Chordwise C.G.Distribution

5. Stiffness and Stiffness Distribution

A computer program was developed to calculate the bending stiffness of the composite blade. In the bending stiffness tests, the bending strains were measured at different radial stations, and the bending stiffness was determined from these measured strains. The tests are shown in Figure 8 and 9.

---

* $\bar{\sigma}e = \dfrac{\int_0^R \bar{m} x_{c.g} dr}{\int_0^R \bar{m} b dr}$, b: *blade chord*

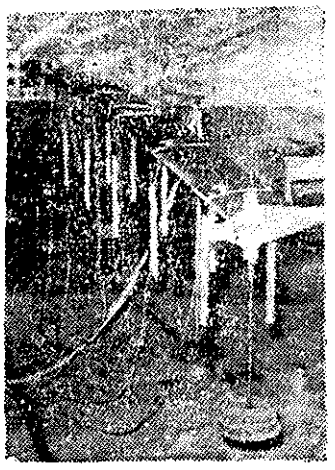

Fig.8 Flapwise Bending Stiffness Test

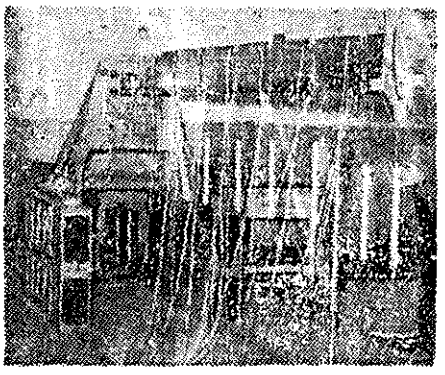

Fig.9 Chordwise Bending Stiffness Test

Figure 10 ond 11 show the calculated and measured values of the bending stiffness. It is seen that the calculated values agree with the measured data, except for the deviation of the measured chordwise bending stiffness data at some stations which may be mainly due to the structural discontinuity at these positions.

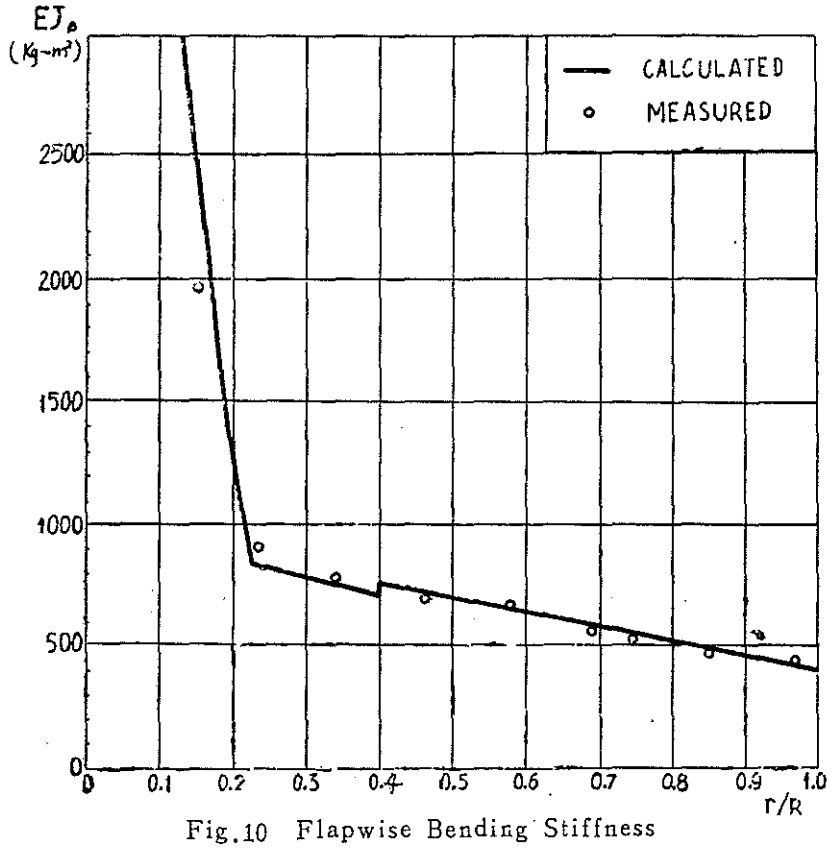

Fig.10 Flapwise Bending Stiffness

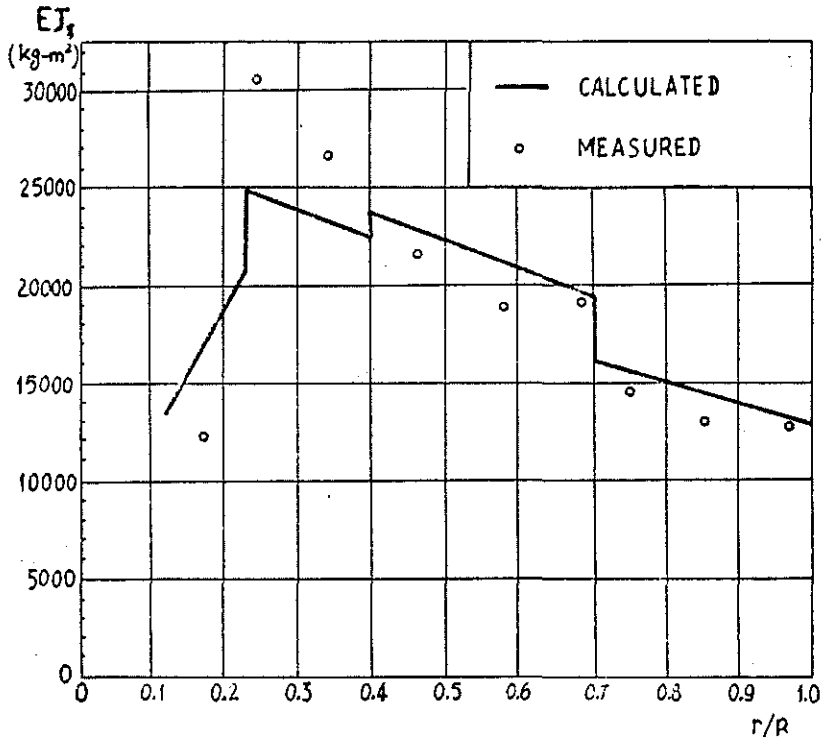

Fig.11 Chordwise Bending Stiffness

From the above results, we find that the blade flapwise bending stiffness is well within the range of values to keep the reguired clearance between blade tip and the helicopter tail cone.

Fig.12 Blade Torsional Stiffness Test

The blade torsional stiffness was measured through a torsional stiffness test, Fig. 12. The torsional displacements at various spanwise stations were measured to determine the torsional stiffness distribution, which is shown in Fig.13.

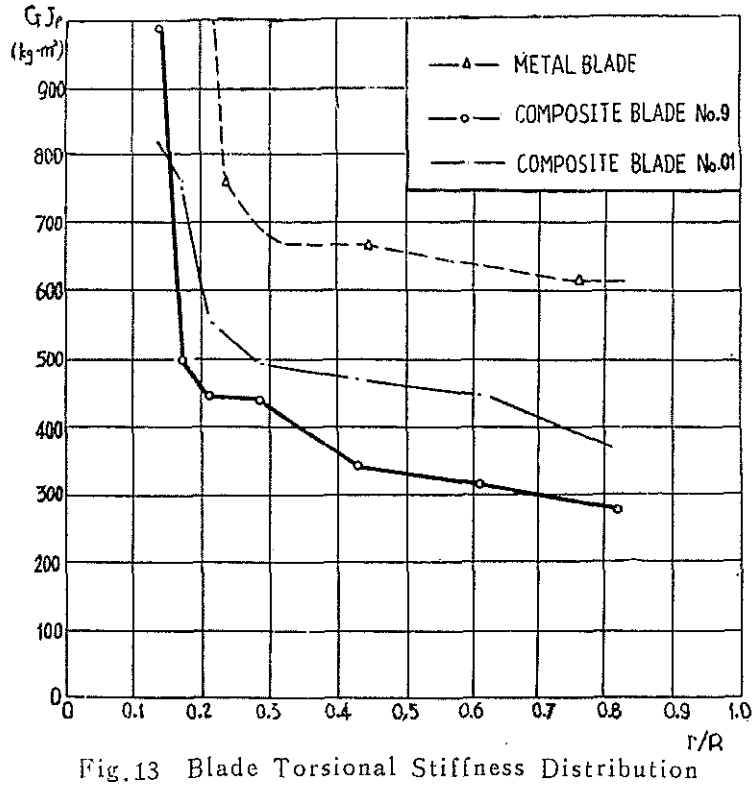

Fig.13 Blade Torsional Stiffness Distribution

The skin of blade No.9 consists of only four layers of glass cloth, and that for blade No.01 is increased to six for the final design. It was found that increasing the thickness of skin has a significant effect on the torsional stiffness.

6. Blade Bending Natural Frequency

The bending natural frequencies of composite blade were calculated by a computer program developed in the design process. The bending stiffness used in the frequency calculation is somewhat higher than the above mentioned static stiffness value due to the difference between the dynamic modulus and the static modulus of composite material.

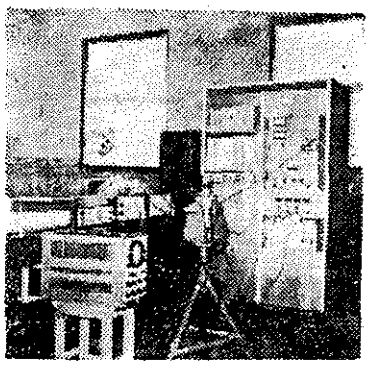

Fig.14 Dynamic Modulus Experiment

An experiment was conducted to

estimate this difference. The dynamic modulus was determined from the measured natural frequency of a specimen cut out from the actual blade, Fig. 14, and the static modulus from the deformation of the same specimen under static load. It is concluded from the experiment that the dynamic modulus is higher than the static modulus by about 10%.

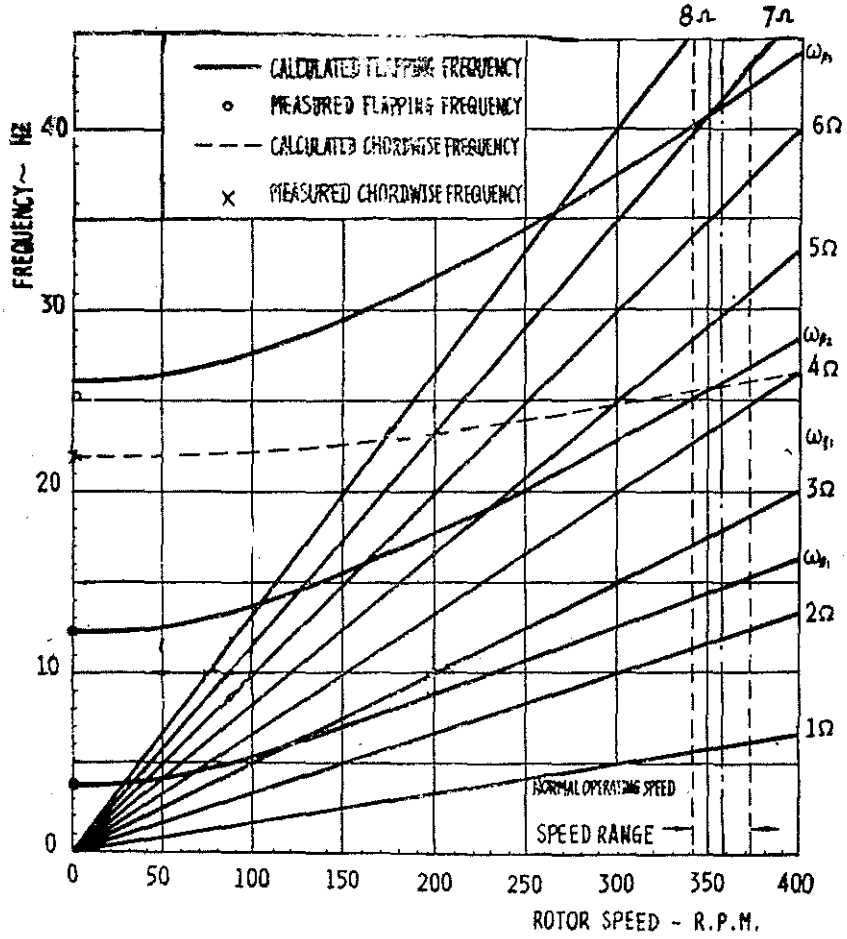

Fig.15 Composite Blade Bending Natural Frequency

This ratio was used in the calculation of the blade natural frequency, with its results shown in figure.15, and the natural frequency ratio at normal operating speed listed in Table.4.

The natural frequency distribution is satisfactory except for the 3rd flapping mode, when it is near resonance at the normal operating speed. It is concluded from the stress calculation and test results that such a situation does not cause any serious blade dynamic stress problem.

Table.4 Blade Natural Frequency Ratio at Normal Operating Speed

	Flapwise			Chordwise	
	$\omega_{\beta 1}/\Omega$	$\omega_{\beta 2}/\Omega$	$\omega_{\beta 3}/\Omega$	$\omega_{\zeta 1}/\Omega$	$\omega_{\zeta 2}/\Omega$
Composite Blade	2.48	4.35	6.92	4.3	11.8
Metal Blade	2.56	4.23	6.65	2.63	5.76

ω: Blade Natural Frequency; Ω: Rotor Rotating Speed

For the lst chordwise bending mode, the natural frequency ratio of blade No. 9 with four layers of skin and fiberglass trailingedge strip is only 3.72. As Mentioned above, the number of skin layers was later increased to six in order to improve the torsional stiffness. Thus, the natural frequency ratio would actually be nearer to 4. Finally, when carbon fiber was used instead of fiberglass for the trailingedge strip, the natural frequency ratio increased to 4.3 and resonance was completely avoided.

Since the environmental temperature has significant effect on the modulus of composite material, the blade natural frequency may be changed to a certain extent due to temperature variation. As our helicopter is expected to be in service under both extremely high and low temperatures (+60℃～45℃), we must consider the change in natural frequency under such environment.

The variation of dynamic modulus vs temperature was measured in an experiment, see figure 16, and its data was subsquently used to calculate the natural frequency at high and low temperatures. It was found that there is no resonance due to the influence of temperature.

The nonrotating natural frequency was measured in the natural

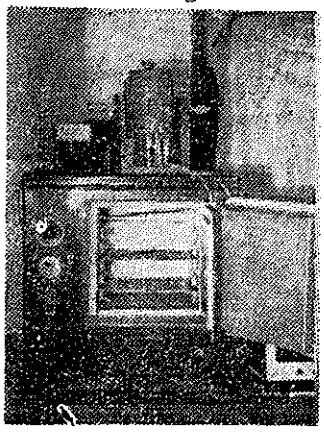

Fig.16 The Experiment to Evaluate the Influence of Temperature on the Dynamic Modulus

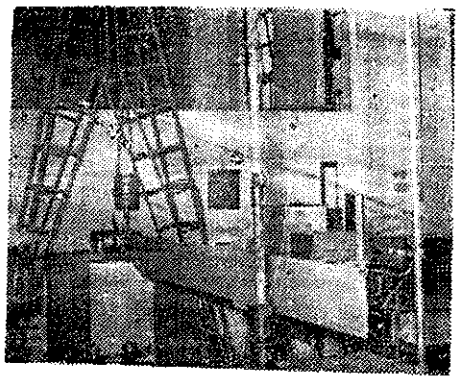

Fig.17 Chordwise Natural Frequency Test

frequency test, Fig. 17, with its data listed in Table. 5 in comparison with the calculated values. The agreement is excellent except somewhat for the 3rd flapping mode, in which the measured value of this mode is lower than the calculated value.

Table.5 Composite Blade Measured and Calculated Nonrotating Natural Frequency

	Flapwise			Chordwise	
	1st Mode	2nd Mode	3rd Mode	1st Mode	2nd Mode
Measured Value, Hz	3.89	12.22	24.96	22.1	63
Calculated Value, Hz	3.83	12.31	26.19	21.97	66.5

A rotating natural frequency test was also conducted in the ground tie-down test. The alternative bending strain was recorded by the tape recorder at various rotor speed. The natural frequency was identified from the frequency spectrum analysis. Although the analysis of the test results has yet to be completed, we can anticipate that the measured 3rd flapping rotating natural frequency would be similar to the nonrotating natural frequency, which is somewhat lower than the calculated value, so that resonance in the operating speed range would not be likely to occur.

7. Rotor-Body Coupled Natural Frequency

For an articulated rotor, the rotor-body coupling effect may have significant influence on the blade chordwise bending natural frequency. From such a consideration, the coupled natural frequency was determined through actual testing and theoretical analysis in the development process. Here, mechanical impedance method was used in the analysis.

One of the coupled modes is the rotor cyclic chordwise bending mode coupled with rotor shaft end longitudinal and lateral vibration. During the development process a method was developed to solve the problem with the nonisotropic character of the rotor support system being taken into account. The longitudinal and lateral impedance at the shaft end were measured individually through impedance tests, Figure 18.

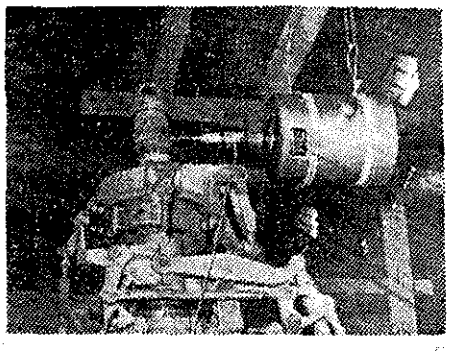

Fig.18 Rotor Shaft End Longitudinal Impedance Test

The impedance of the rotor cyclic mode at the rotor center was determined analytically. The rotor-

body combined impedance curves are shown in Figure. 19, where the horizontal coordinate is the frequency in the nonrotating system. The coupled natural frequencies are determined from the coincidence of curve A with A_1, A_2, such as point B, C, D, E. The coupled natural frequencies at normal operating speed are listed in Table. 6.

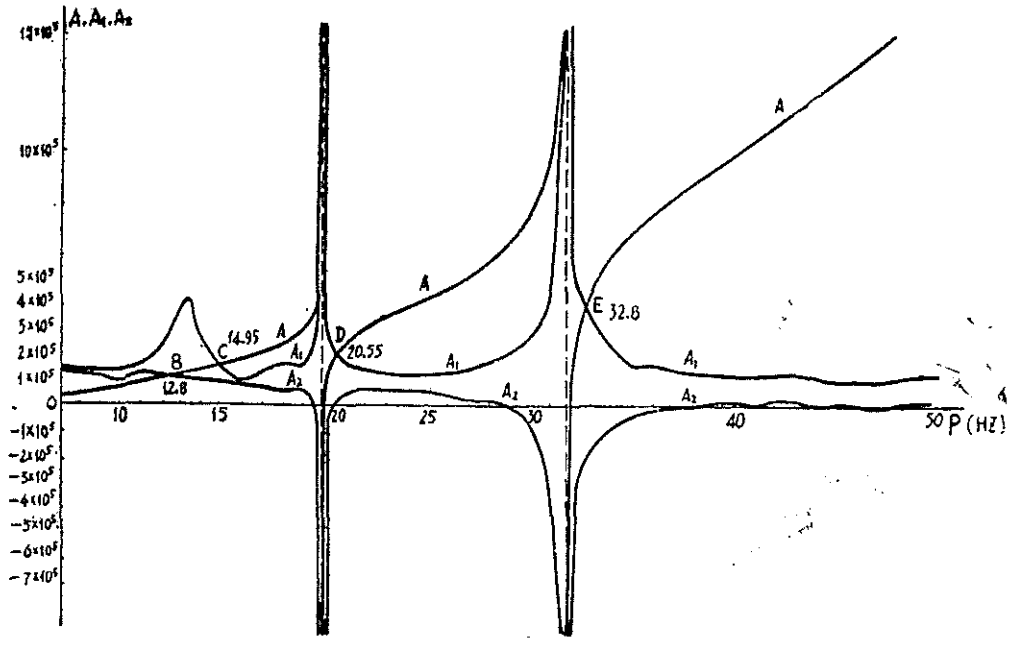

Fig.19 Rotor-Body Combined Impedance Curves (Normal Speed)

Table.6 Rotor Cyclic-Lag-Mode/Body Coupled Natural Frequency

Coincident Point	Natural Frequency at Nonrotating System		Natural Frequency at Rotating System		
	P_F, Hz	P_F/Ω		P_R, Hz	P_R/Ω
B	12.8	2.146	P_1	18.765	3.146
			P_2	6.835	1.146
C	14.95	2.506	P_1	20.915	3.506
			P_2	8.985	1.506
D	20.55	3.445	P_1	26.515	4.445
			P_2	14.585	2.445
E	32.8	5.499	P_1	38.765	6.499
			P_2	26.835	4.499

Let P_F be the coupled natural frequency in the nonrotating system, i.e., the body frequency, P_R be the natural frequeucy in the rotating system, i. e., the blade chordwise bending frequency, $P_1=P_F+\Omega$, be the regressive mode frequency, $P_2=P_F-\Omega$, be the advancing mode frequency. It is evident that due to the nonisotropic character of the rotor support system, i. e., the shaft end longitudinal impedance is not equal to the lateral impedance, there are two rotor modes in every coupled mode. It is interesting to note that the isolated 1st chordwise bending mode frequeucy is 25.82 Hz, and from Table.6 P_1 of coupled mode D is 26.515 Hz, P_2 of coupled mode E is 26.835Hz, so the coupling effect is not negligible.

It is concluded from Table.6 that as P_F is not coincident with 3Ω, 6Ω···etc, there is no resonance for the coupled modes.

Another coupled mode is the rotor collective chordwise bending mode coupled with the rotor shaft end torsional vibration. In order to obtain the coupled natural frequency, the torsional impedance of the total transmission system at the rotor shaft end was determined analytically. The impedance of rotor collective mode at rotor center was also determined analytically. The impedance curves are shown in Figure.20.

The coupled natural frequencies are listed in Table.7.

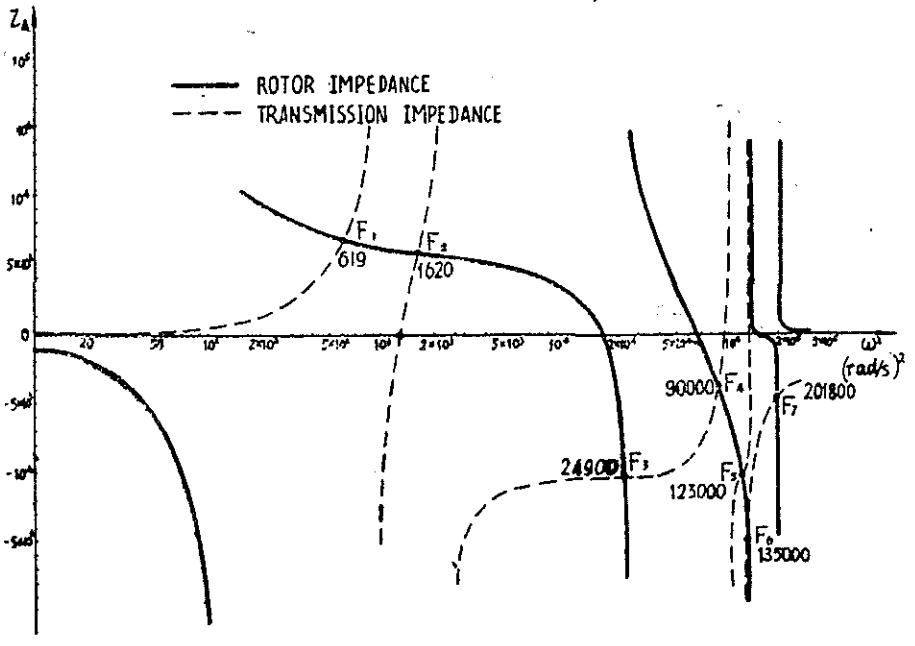

Fig.20 Rotor Chordwise Collective Mode Impedance and Rotor Shaft End Torsional Impedance

Table.7 Rotor Collective-Lag-Mode/Transmission Coupled Natural Frequency

Coincident Point	P (Hz)	P/Ω
F_1	3.96	0.664
F_2	6.41	1.075
F_3	25.11	4.210
F_4	47.75	8.005
F_5	55.82	9.358
F_6	58.41	9.792

P is not coincident with 3Ω, 6Ω…etc, so there is no resonance for this coupled mode. The coupled natural frequency of F_3 is 25.114Hz. Compared with the isolated frequency 25.82Hz, it is evident that the coupling effect is also not negligible.

8. Blade Torsional Natural Frequency

The blade torsional vibration is coupled with the control system vibration (collective pitch control system and cyclic pitch control system respectively). The mechanical impedance method was also used to solve this problem. The impedance of the control system was measured through tests. The impedance of the blade torsional vibration at blade root end was determined analytically. The results are shown in Table. 8.

Table.8 Blade Torsional Natural Frequency

	Coupled with Collective Pitch Control System	Coupled with Cyclic Pitch Control System	
		Advancing Mode	Regressive Mode
Natural Frequeucy ω (Hz)	20.05	19.42	22.41
Frequency Ratio ω/Ω	3.36	3.26	3.76

9. Flight Loads Prediction

During the development process, blade loads were calculated. The results are shown in Figure. 21, 22 and 23.

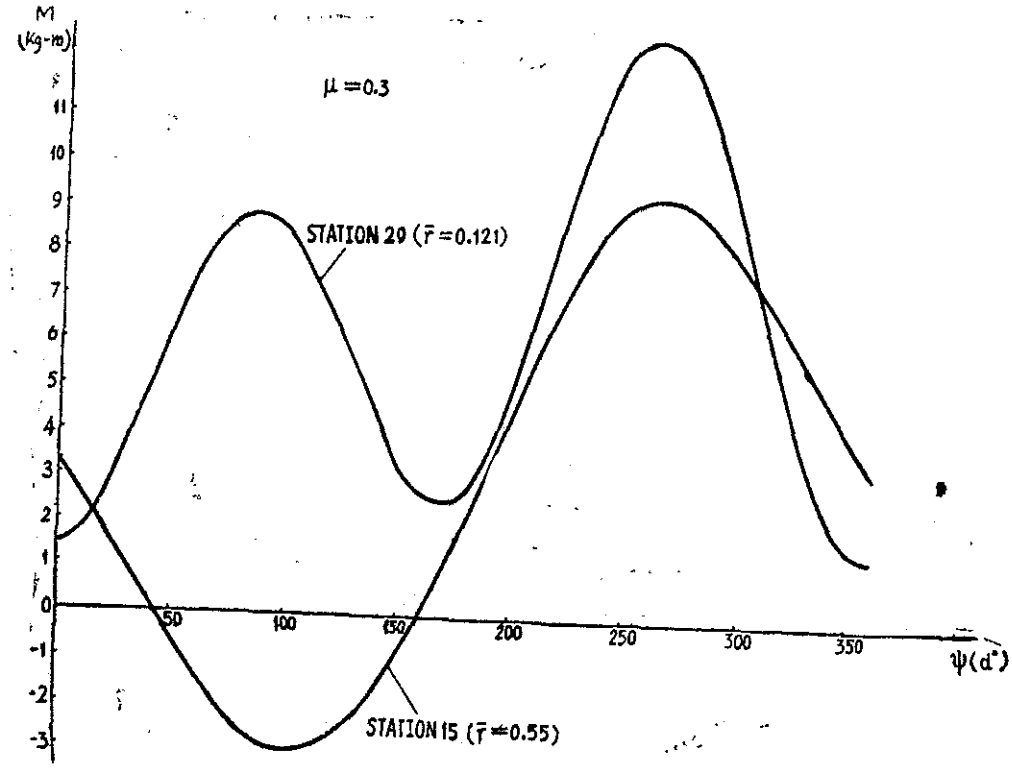

Fig.21 Flapwise Bending Moment vs. Azimuth

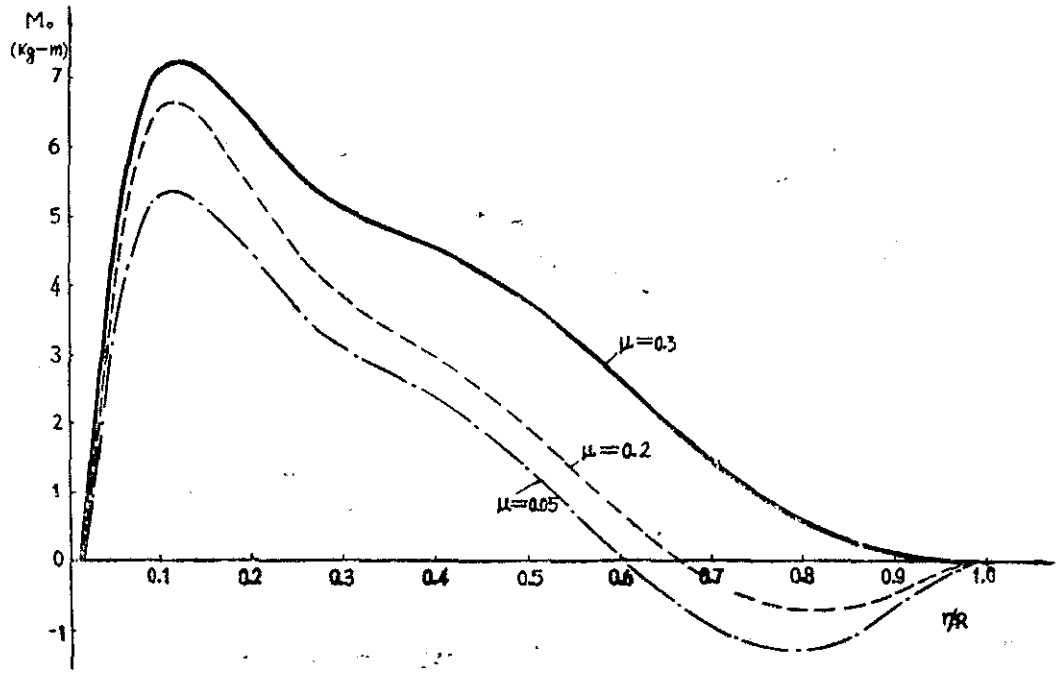

Fig.22 Steady Bending Moment Distribution

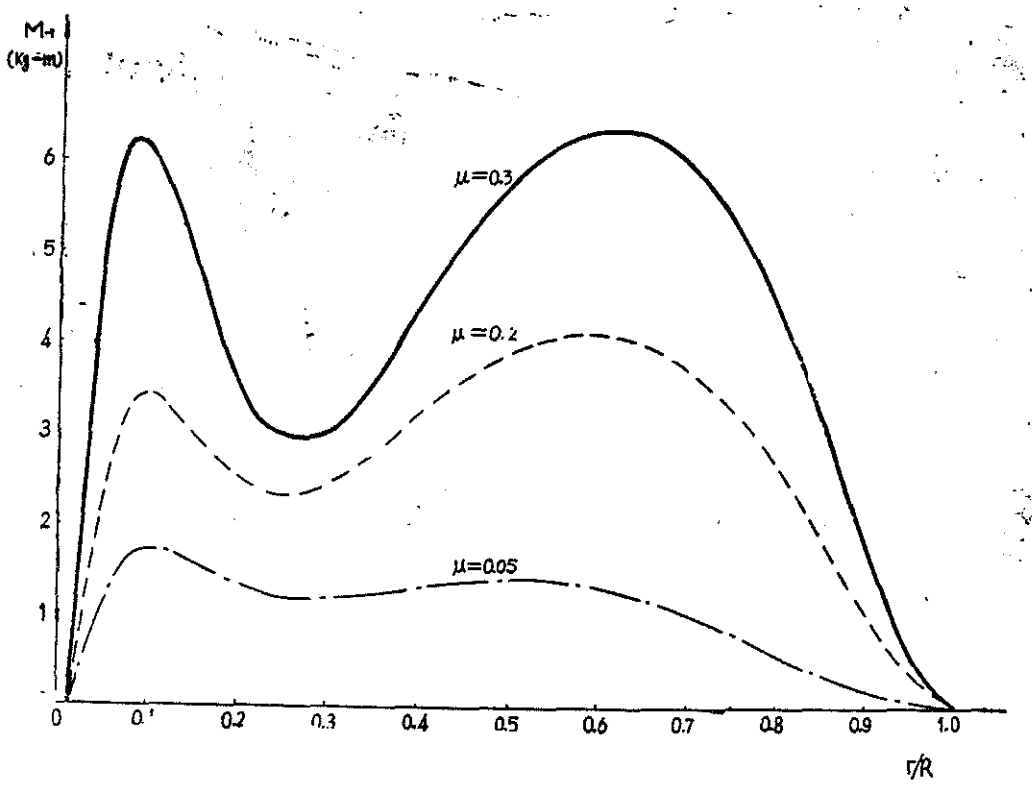

Fig.23 Oscillatory Bending Moment Distribution

10. Static Proof test

Static proof tests include blade root section tensile test, full scale blade flapwise bending test and chordwise bending test.

In the blade root tensile test the specimen was subjected to an axial tensile load to simulate ultimate centrifugal load, see Figure.24. The design ultimate load is 28.9 tons. When the tensile load reached 56.6 tons, shear failure occured at the blade-hub connecting bolt, and the test was stopped.

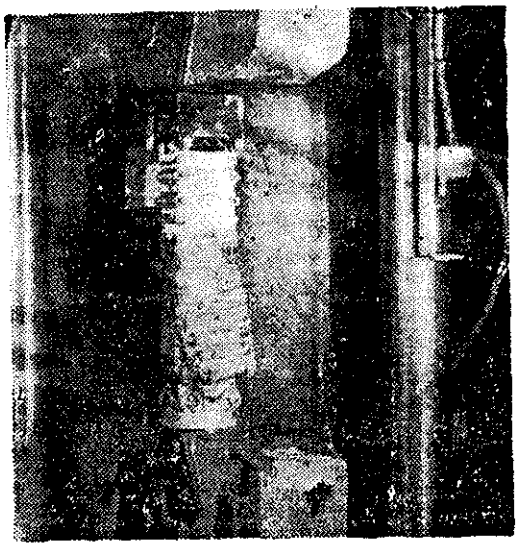

Fig.24 Blade Root Tensile Test

The flapwise and chordwise bending test are shown in Figure 25 and 26. In these tests the blade was tested up to the limit load without any failure (including trailing edge buckling) or detectable residual deformation.

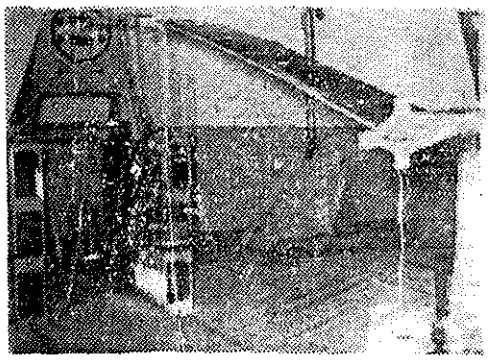

Fig.25 Flapwise Bending Test

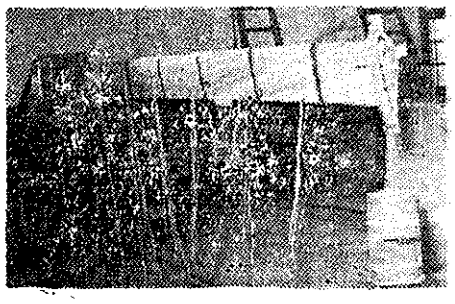

Fig.26 Chordwise Bending Test

11. Fatigue Test

The purpose of the blade section fatigue test is to determine the blade fatigue strength, i.e. the S-N curve of the component. Using the S-N curve together with the flight load, the blade fatigue life can be determined by the cumulative damage theory.

Due to the high centrifugal force and strong structural discontinuity, the blade root end is the most critical part of the blade. Root end fatigue test was conducted during the development process. The test specimen was cut out from a full scale blade, see Figure. 27. Test loads are listed in Table. 9.

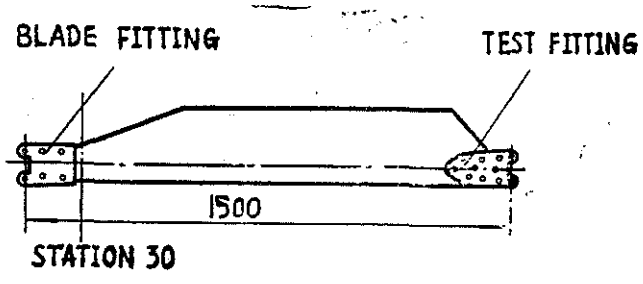

Fig.27 Root End Fatigue Test Specimen

Table.9 Blade Root End Fatigue Test Loads

Axial Load (Centrifugal Force)	kg	9000
Chordwise Alternative Bending Moment	kg-m	±25.2
Flapwise Alternative Bending Moment at Station 30	kg-m	±160
Corresponding Flapwise Alternative Bending Strain at Station 30	$\mu\varepsilon$	1050

The chordwise alternative bending moment is equal to 120% of the friction damper damping moment, which is constant for any flight condition.

The test stand is shown in Figure. 28. The specimen is excited by electro-hydraulic servo controlled actuator at the resonance frequency of the specimen (~22Hz). The chord line of the specimen is inclined at a certain angle to produce chordwise bending moment.

Fig.28 Fatigue Test Stand

Three specimens were tested in the program. Fatigue cracks were present in the metal fittings from ~1×10^6 cycles to ~6×10^6 cycles, see Figure. 29. The metal fittings were changed and the test was continued. All of the three specimens was tested to 2×10^7 cycles. There was no fatigue failure present at the composite structure.

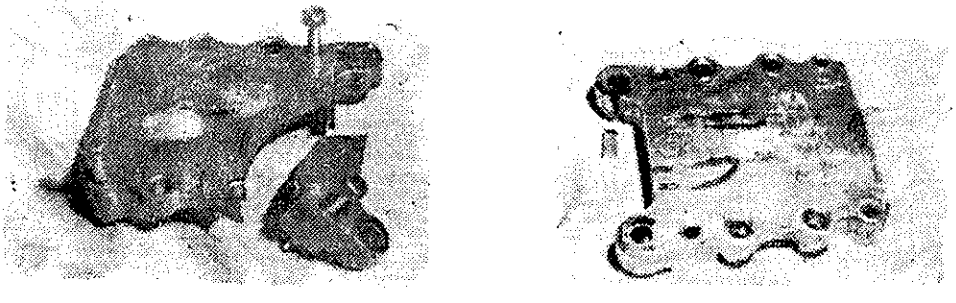

Fig.29 Fatigue Failure of the Blade Metal Fitting

As the flapwise alternative bending moment used in the fatigue test is about 2/3 of the flapwise static limit load, the test result shows an extremely high fatigue strength of the blade root end.

Blade root end S-N curve was derived from the test data and material S-N curve shape factor. Due to the lack of measured flight loads, the blade fatigue life cannot be determined at the present stage. Compared with the above mentioned calculated flight load, an extremely high fatigue life is anticipated.

12. Ground Tie-down Test

During the helicopter tie-down test the blade tracking was conducted and the blade rotating natural frequency was measured. Only a small amount of pitch link rod adjustment is required to make the blade track

within the tolerable range. This fact shows the similarity of the blades in aerodynamic and dynamic properties.

20 test hours were accumulated in the program. There is no failure or debonding detected on the blade.

Fig.30 Ground Tie-down Test

13. Conclusion

Through the design and development project, it is concluded that the new composite blade just developed is much superior to the original metal blade in all aspects of our investigation, and the basic requirements set out at the beginning of the project are completely satisfied. We expect the experimental techniques and theoretical methods developed in carrying out this project could be used as a background for further development.

14. Acknowledgement

The authors are grateful to Professor Zheng Zhaoquan for his dedication in completing the English manuscript of this paper.

15. Reference

Guo Zehong, Gu Zhongquan, Zhang Lingmi, Liu Shoushen: The Development and Tests of Yan'an 2 Light Helicopter.
Presented at the Eighth European Rotorcraft Forum, Aix-en-provence, France, August 31 — September 3, 1983.